Biosensors and Bioelectronics 133 (2019) 48–54

Contents lists available at ScienceDirect

Biosensors and Bioelectronics

journal homepage: www.elsevier.com/locate/bios

Carbon dots stabilized silver–lipid nano hybrids for sensitive label free DNA detection

Karutha Pandian Divya[a,b], Rangasamy Karthikeyan[c], Bharathi Sinduja[c], Arockiajawahar Anancia Grace[a,b], S. Abraham John[c], Jong Hoon Hahn[d], Venkataraman Dharuman[a,*]

[a] Molecular Electronics Laboratory, Department of Bioelectronics and Biosensors, Science Campus, Alagappa University, Karaikudi 630003, India
[b] Department of Industrial Chemistry, Alagappa University, Karaikudi 630003, India
[c] Centre for Nanoscience and Nanotechnology, Department of Chemistry, The Gandhigram Rural Institute, Gandhigram 624302, Tamil Nadu, India
[d] Department of Chemistry and BioNanotechnology Center, Pohang University of Science and Technology, San 31, Hyojadong, Pohang 790-784, South Korea

ARTICLE INFO

Keywords:
Carbon dots
Silver
Nanoparticle
Monolayer
Liposome
Label free
DNA
Sensing

ABSTRACT

Carbon dots have been extensively used for the development of fluorescent based molecular affinity sensors. However, label free DNA sensing by electrochemical method is not reported so far. Herein, we report carbon dots stabilized silver nanoparticles (CD-AgNPs) lipid nano hybrids as a sensitive and selective platform for label free electrochemical DNA sensing. The CD-AgNPs were synthesized by wet chemical method and then characterized by UV-visible, Fourier-transform Infra-red (FT-IR), dynamic light scattering (DLS) and high resolution transmission electron microscopy (HR-TEM) techniques. These CD-AgNPs were used for decorating the binary lipid 1,2-dioleoyl-*sn*-glycero-3-phosphoethanolamine (DOPE) and N-[1-(2,3-Dioleoyloxy)propyl]-N,N,N-trimethylammonium chloride (DOTAP) surface (named as lipid) and tethered on self-assembled monolayer of 3-mercaptopropionic acid (MPA) (MPA-lipid-CD-AgNPs). The formation of array of MPA-lipid-CD-AgNPs on Au electrode was confirmed by atomic force microscopy (AFM). Electrochemical behavior of MPA- lipid-CD-AgNPs was monitored in the presence of 1 mM potassium ferri/ferrocyanide (K_3/K_4 [$Fe(CN)_6$]). The formation of layer-by-layer MPA-lipid-CD-AgNPs is indicated by increased anodic and cathodic peak (ΔE_p) separation with decreased redox peak current of K_3/K_4 [$Fe(CN)_6$]. Short chain DNA (30 mer oligonucleotide, representing the lung cancer) was used as a model system for label free DNA sensing. Un-hybridized (single stranded DNA), hybridized (complementary hybridized), single, double and triple base mismatched target DNA hybridized surfaces were efficiently discriminated at 1 μM target DNA concentration at the Au/MPA-lipid-CD-AgNPs electrode by change in the charge transfer resistance from impedance technique. Further, the modified electrode was successfully used to determine target DNA in a wide linear range from 10^{-16} to 10^{-11} M. The present work open doors for the utilization of CDs in molecular affinity based electrochemical sensor design and development.

1. Introduction

Development of selective and sensitive molecular affinity sensors for the early detection of cancer is important to improve diagnosis and preventive care in order to reduce the mortality rate. Fluorescene, surface plasmon resonance and electrochemical based biomarker detection methods have been reported for the early detection of cancer. In the fluorescence based biosensing, cyanine based organic fluorophore dye (either cy3 or cy5) is attached to the target DNA. Hybridization of fluorescent labeld complementary target DNA (cDNA) with the pre-immobilized single stranded DNA (ssDNA) on the surface (called as hybridized surface) exhibits fluorescence signal proportional to the target DNA concentration. Absence of fluorescence for the control surface (non-complementary target DNA hybridized surface, named as un-hybridized) under identical experimental condition indicates high selectivity and sensitivity of the sensor developed. Alternatively, fluorescence quenching method is also developed in parallel for detecting the DNA and proteins (Zhang et al., 2013a; Jans and Huo, 2012; Yang et al., 2013; Tian et al., 2017). Nanomaterials like gold nanoparticles (AuNPs) (Wilson, 2008; Li and Rothberg, 2004), carbon nanotubes (CNTs) (Yang et al., 2008; Chen et al., 2011), graphene oxide (GO) (Lu et al., 2009; Li et al., 2013), MoS_2 (Huang et al., 2015; Zhu

* Corresponding author.
E-mail address: dharumanudhay@yahoo.com (V. Dharuman).

https://doi.org/10.1016/j.bios.2019.03.027
Received 14 January 2019; Received in revised form 14 March 2019; Accepted 14 March 2019
Available online 15 March 2019
0956-5663/

et al., 2013) and g-C_3N_4 nanosheets (Wang et al., 2013; Yang et al., 2015; Ping et al., 2015) are used as transducers to quench the fluorescence from the dye-labeled target DNA molecule through Fröster Resonance Energy Transfer (FRET) processes.

Carbon dots with size lesser than 10 nm (Xu et al., 2004) with high chemical stability, electronic, optical and easy surface functionalization properties, low cost and low toxicity (Yang et al., 2012; Shen et al., 2012; Ray et al., 2009; Tang et al., 2012) are finding applications in catalysis (Zhu et al., 2012), sensors (Yu et al., 2015), supercapacitors (Y.R. Zhu et al., 2013), bioimaging (Bhunia et al., 2013; Chen et al., 2013) and drug delivery (Kim et al., 2013; Zheng et al., 2014; Cailotto et al., 2018). Development of FRET biosensor using carbon dots is an evergreen field for the fact that the fluorescence property of carbon dots originates from the inter band transitions between the conjugated π-domains and surface defects (H. Li et al., 2011). In this method, the dye labeled DNA is adsorbed in parallel orientation on the carbon dot by π–π interaction (Sheila and Gary, 2010; Varghese et al., 2009). The close proximity between the fluorescence dye and carbon surface induces FRET and quenches the fluorescence signal. Hybridization with the complementary target DNA releases the fluorophore and induces fluorescence signal (H. Li et al., 2011). Further, detection signal enhancement is made using acid functionalized CDs for anchoring large amounts of DNA (Loo et al., 2016) and human IgG (Zhu et al., 2014) capture probes. Similarly, amine (Kudra et al., 2017) and polyethyleneimine functionalized CDs are also reported for DNA damage detection (Dou et al., 2015). In another method, electron resonance property of metal is coupled with the emission property of CDs for the improved fluorescence activity (Wang et al., 2014) and applied for the Surface Enhanced Raman Spectroscopy (SERS) (Luo et al., 2012), biomedical (Kleinauskas et al., 2013; Mao et al., 2014) and catalytic (Mondal et al., 2014; Yu et al., 2012) based sensing applications.

Among the metals studied, silver nanoparticles have gained interest due to their distinctive size, shape relative antimicrobial activities, stability, optical, catalytical (El-Sayed, 2001; Wang et al., 2011; Halder et al., 2011; Zhang et al., 2011; Sharma et al., 2009) and excellent SERS properties (Zhang et al., 2013b). The strong luminescence property of CDs has been successfully used to sense several biomolecules and metal ions based on their luminescence quenching (Sun and Lei, 2017). Recently, synthesis of CD-AgNPs nanocomposite and its antibacterial activity (Wang et al., 2017) and application towards non-enzymatic electrochemical sensing of H_2O_2 (Jiang et al., 2014) are reported. The CD-Ag@ZnO core shell nanocomposite is studied for the cellular uptake and apoptosis (Sachdev et al., 2015). CDs photoluminescent property is enhanced by making a composite Ag/SiO_2 layer assembly (J. Li et al., 2011).

Although fluorescence based sensor is more sensitive and selective, it is expensive and has the difficulty of miniaturization which is a critical requirement for portable device development. Further, these sensors show high non-specific signal generation due to the uncontrolled and improper probe orientation resulting from the π-π electron interactions between DNA and CDs. Recently, CDs are used as fluorescent probe for the recognition of base pair selective and sequence specific DNA (Guo et al., 2018; Pramanik et al., 2018). However, to the best of our knowledge no report is available in the literature for the detection of DNA using CDs composite with noble metal nanoparticles. Thus, the objective of the present study is to synthesize CD-AgNPs and utilize them for the label free electrochemical detection of DNA after modified on Au electrode self-assembled with MPA. The label free DNA hybridization detection without using fluorescence or enzyme labels is the most prominent approach in the construction of low-density DNA microarrays for various applications including medical diagnosis (Ostatna and Palecek, 2006; Mao et al., 2009; Tiwari and Gong, 2009), warfare agent detection (Ivnitski et al., 2003), food quality control (Lermo et al., 2007; Cagnin et al., 2009) and environmental monitoring (Palchetti and Mascini, 2008). However, the electrochemical label free detections suffer from poor selectivity and sensitivity due to poor orientation and arrangement of DNA on the transducer surfaces as well as poor reproducible and inconsistent data. Despite the development of numerous methods for controlling the orientation of the immobilized single stranded DNA on the electronic transducers, complete control of the orientation is still questionable. In this aspect, liposome vesicle is used for anchoring single stranded DNA in few reports (Alfonta et al., 2001). However, both biotin-avidin interactions and covalently linked enzyme labels were used for electrochemical signal amplification following the target DNA hybridization (Wang et al., 2014). To the best of knowledge, no work is available on the use of lipid-carbon dot metal nanoparticle composite for biosensing in the literature till now. Hence, in the present work, the CD-AgNPs is used to decorate the lipid vesicle to form a composite and named as lipid-CD-AgNPs. The lipid-CD-AgNPs was tethered on the MPA monolayer by simple electrostatic interaction on Au electrode which was confirmed by cyclic voltammetry and electrochemical impedance spectroscopy. Label free selective and sensitive DNA detection is demonstrated using commercially obtained lung cancer DNA sequence as a model system. For this, the thiolated single stranded DNA is immobilized covalently on the MPA- lipid-CD-AgNPs surface. The hybridization with complementary, non-complementary and base mismatched target DNAs were made for demonstrating the selectivity. Tethering of lipid- CD-AgNPs composite by layer-by layer assembly and label free DNA detection method developed are simple, fast and sensitive to molecular affinity reaction.

2. Experimental section

2.1. Materials

Potassium ferrocyanide, potassium ferricyanide, potassium chloride, sodium chloride, sodium hydroxide, monosodium phosphate, hydrochloric acid and sodium borohydride were purchased from Himedia, India. 3-mercaptopropionic acid was procured from Sisco Research Laboratory, India. 1, 2-dioleoyl-*sn*-glycero-3-phosphoethanolamine (DOPE), N-[1-(2,3-Dioleoyloxy)propyl]-N,N,N-trimethylammoniumchloride (DOTAP), silver nitrate and L-asparagine were procured from Sigma-Aldrich, USA. 30-mer lung cancer synthetic oligonucleotides were synthesized by MWG biotech, Ebersberg, Germany, with HPLC purification. The following sequences were used:

Capture probe (ssDNA): 5′- HS-$(CH_2)_6$ – *ATC ACA GAT TTT GGG CGG GCC AAA CTG CTG-3′*- I
Complementary target (cDNA): 5′- *CAG CAG TTT GGC CCG CCC AAA ATC TGT GAT-3′*- II
Non-complementary target (ncDNA): 5′- *TGA TGA CCC AAT TTA TTT GGG GCT CAC AGC -3′*-III
Single base mismatch target (smmDNA): 5′- *CAG CAG TTT GGC CTG CCC AAA ATC TGT GAT -3′*- IV
Double base mismatch target (dmmDNA): 5′- *CAG CAC TTT GGC CTG CCC AAA ATC TGT GAT -3′*- V
Triple mismatch target (tmmDNA): 5′- *CAG CAC TTT GGC CTG CCC AAA AGC TGT GAT -3′*- VI

2.2. Methods

The Au working electrode was cleaned for 1 h in piranha solution, polished with Al_2O_3 powders (5.0, 1.0 and 0.05 μm) and sonicated in milli-Q water for 10 min. The saturated calomel reference electrode, Pt wire counter electrode and modified Au working electrode were used in the three electrode system. The electrochemical measurements were carried out by using 605D-CH Instruments, Texas, USA. The impedance measurements were made in the frequency range 100 MHz to 0.1 Hz by applying AC potential amplitude ± 5 mV over the DC potential 160 mV (redox potential of $K_3/K_4[Fe(CN)_6]$ in PBS) and the data are presented in the form of Nyquist plot. Zsimpwin software was used to simulate the experimental data using the equivalent circuit $[R_s(Q_{dl}(R_{CT}W))]$ in

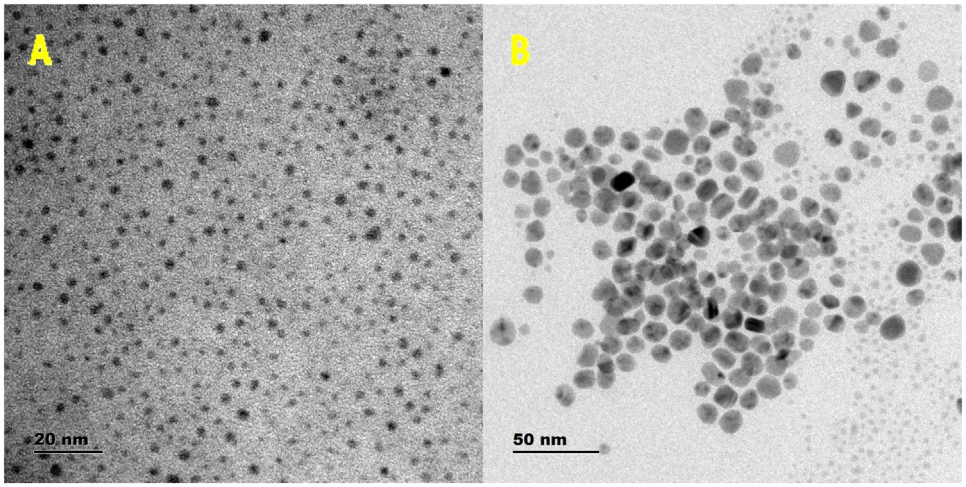

Fig. 1. HRTEM images of (A) CDs and (B) CD-AgNPs.

which R_s refers to solution resistance, Q_{dl} and R_{CT} represents the constant phase element and charge transfer resistance of the gold electrode, respectively, and W refers to the Warburg element. The constant phase element (Q_{CPE}, F cm^{-2}) is used in place of capacitor C to account for the high roughness of the surface. The impedance, Z(ω), of the Q_{CPE} is given by the following equation

$$Z(\omega) = \frac{1}{Q_{CPC}(j\omega)^n}$$

CPE component is roughly equal to the specific capacity of the electrode/solution interface. The angular frequency ω is equal to 2πf, where f is the frequency. The dimensionless CPE exponent 'n' is directly related to the degree of the surface roughness and inhomogeneity of the electrode surface that varies between 0.5 and 1. In case of a pure capacitor, the value of n is equal to 1 for ultra smooth electrode surface like mercury. The value of $0.5 < n < 1$ indicates the presence of surface roughness and the inextricability of Q_{CPE} from the equivalent circuit. The AFM images and histogram were recorded using NTMDT, NTEGRA Prima, Russia in tapping mode using a gold chip. The HR-TEM images were recorded using FeiTecnai G2 20 twin (USA make) using carbon coated copper grid. UUV-Visble data were recorded using Jasco V850 instrument. FTIR spectrum were recorded using Jasco FT IR 4500 instrument. Quantification of DNA concentration was done using the Nanospectrophotometer instrument, Biospec-Nano, Shimadzu make, Japan.

2.3. Synthesis of carbon dots and carbon dots capped silver nanoparticles

The precursor L-asparagine was used to prepare CDs. 0.5 g of L-asparagine was heated in a heating mantle at 100 °C. After 10 min, it was liquated and within 20 min the colorless solution was changed to brown. This brown color solution was diluted by adding 50 mL of 10 mg/mL NaOH (Gowthaman et al., 2017). The carbon dots capped silver nanoparticles (CD-AgNPs) were prepared by reducing 0.5 mL silver nitrate solution using 0.1 mL of $NaBH_4$ in 9 mL milli-Q water containing 0.2 mL of CDs solution.

2.4. Immobilization of liposome-carbon dots capped silver nanoparticles on gold transducer and DNA sensing

Stock solutions of each liposome N-[1-(2,3-Dioleoyloxy)propyl]-N,N,N-trimethylammoniumchloride (DOTAP) and 1,2-dioleoyl-*sn*-glycero-3-phosphoethanolamine (DOPE) were prepared by dissolving them in chloroform at the ratio 1:3, dried and rehydrated with buffer solution (pH 7.4) for three times and sonicated for 15 min. The prepared stock solutions were stored at 4 °C until use. The lipid-CD-AgNPs complex was obtained by mixing equal ratio of DOPE, DOTAP and CD-AgNPs and sonicated for 15 min. Since the direct interaction of vesicles lead to the rupture and bilayer formation on the bare gold electrode, short chain MPA is used as the molecular cushion for anchoring lipid-CD-AgNPs on the gold electrode. Concisely, the cleaned Au electrode was immersed in 1 mM MPA in PBS for an hour and washed with PBS to remove the unadsorbed thiol molecules. 2 µL of lipid-CD-AgNPs complex was drop-casted on the pre-formed MPA layer and incubated for 1 h and washed with the PBS. DNA hybridization sensing was made by immobilizing the thiolated ssDNA probe (Capture probe-I, 1 µM of 2 µL DNA in 1 M NaCl, pH 7.0) onto the pre-formed lipid-CD-AgNPs surface under humid conditions and washed using the PBS to remove the unreacted ssDNAs. 1 µM of 2 µL target DNAs (either II, III, IV, V or VI) in 4 × SSC buffer was hybridized on the MPA- lipid-CD-AgNPs-ssDNA anchored surface for 1 h to allow maximum hybdrization events on the solid surface immobilized ssDNA (Peterson et al., 2001; Steel et al., 2000).

3. Results and discussion

3.1. Characterization of carbon dots-silver nanoparticles composite

The prepared CDs and CD-AgNPs are characterized by different techniques. The UUV-visble absorption spectra recorded for CDs, AgNPs and CD-AgNPs are shown in Fig. S1. CDs show an absorption band at 203 nm corresponding to π-π* transition. The AgNPs showed a peak at 421 nm. In the case of CD-AgNPs, the absorbance band was blue shifted to 387 nm due to π-π transition in CD and Ag. Fig. 1A shows the HR-TEM image of CDs. It shows the presence of quasi-crystalline CDs with an average particle size of 1.64 nm, while the DLS showed particle size of 22 nm. The obtained particle size difference between DLS and HR-TEM measurements is related to the fact that while DLS measures the average size of hydrated particles, the HRTEM measures exact size of the nanoparticle. Fig. 1B shows the HR-TEM image of CD-AgNPs. It shows a well defined spherical shaped particles with an average particle size of 5.4 nm. Association of AgNPs with CDs is again confirmed by the elemental analysis (Fig. S2) showing negligible amount of copper impurity. The selected area electron diffraction (SAED) with the absence of rings for CDs (Fig. S3A) confirms its amorphous nature, while the presence of diffraction rings in the SEAD pattern of CD-AgNPs (Fig. S3B) corresponds to the crystalline planes of face-centered-cubic (fcc) structured AgNPs confirming the crystalline nature of CD-AgNPs.

The FT-IR spectra of CDs and CD-AgNPs are shown in Fig. S4. The broad band at 3442 cm^{-1} indicates the presence of amine and hydroxyl groups originated from the precursor, asparagine. The CH_2 stretching

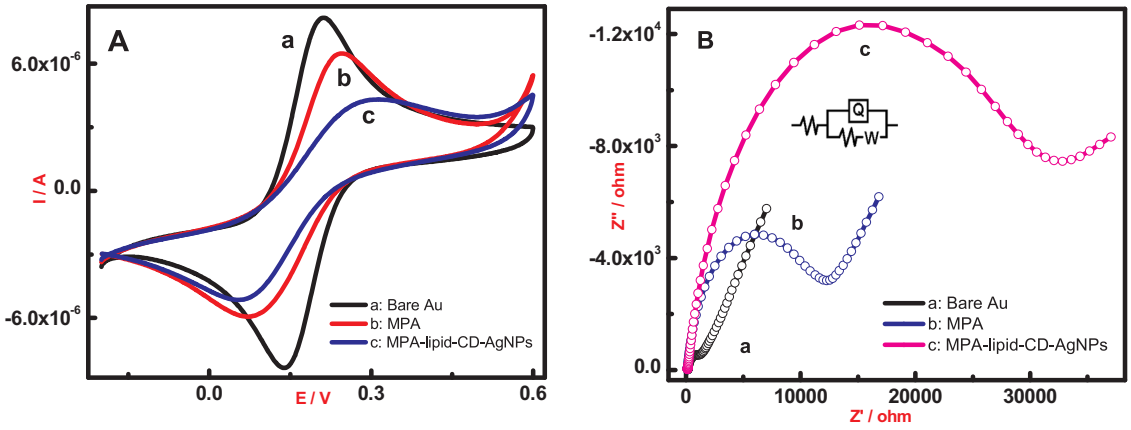

Fig. 2. (A) CV behaviors of bare Au (curve a), MPA (curve b) and lipid-CD-AgNPs (curve c) recorded at a scan rate 50 mVs^{-1} in PBS (pH 7.4) in presence of 1 mM $K_3/K_4[Fe(CN)_6]$.(B). EIS behaviors of MPA (curve a) and lipid-CD-AgNPs (curve b) recorded in the frequency range 100 MHz to 0.1 Hz at an applied DC potential 160 mV in PBS (pH 7.4). The [R(Q(RW)] circuit fit data is given as open circles.

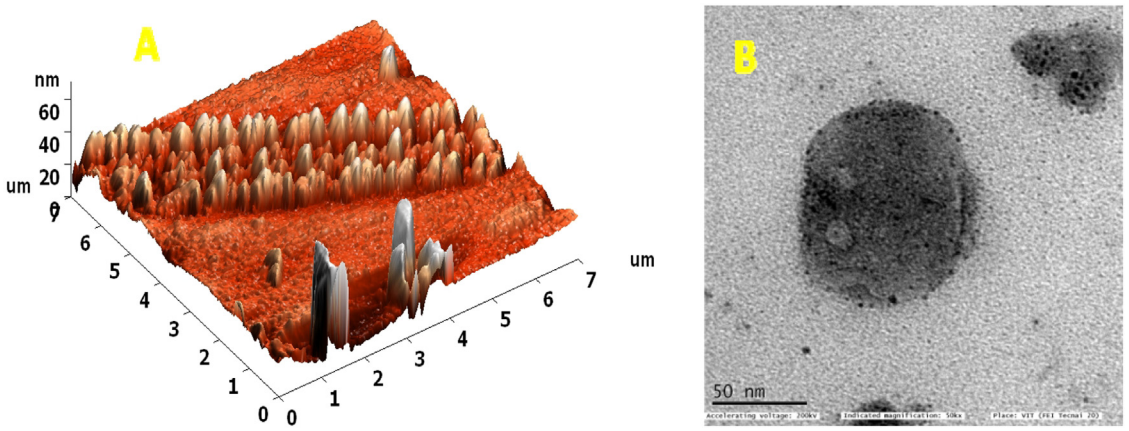

Fig. 3. (A) AFM image of lipid-CD-AgNPs attached on the MPA monolayer presorbed on gold surface. (B) HRTEM image of lipid-CD-AgNPs.

band is indicated by the peaks at 2918 cm^{-1} and 2841 cm^{-1}. The sharp band at 1627 cm^{-1} corresponds to the carbonyl stretching of amide functional group. The band at 1440 cm^{-1} arises from the –N-H deformation mode of –N-H bending. The appearance of band at 1373 cm^{-1} is attributed to the –OH bending of carboxylic acid whereas the band at 1021 cm^{-1} corresponds to –C-N bond stretching of primary amine. The –C-O stretching of carboxylic group is attributed by the peak at 1113 cm^{-1}. The carbonyl stretching of amide functional group at 1627 cm^{-1} and hydroxyl group peak at 3442 cm^{-1} recedes due to the breaking of C=O and H-O bond during the formation of carbon dot capped silver nanoparticle (Jiang et al., 2014).

3.2. Electrochemical behavior of carbon dot capped silver nanoparticle–lipid composite

Gold electrode modified with MPA is used to anchor the lipid-CD-AgNPs. Fig. 2A shows the CV behaviors recorded for different modified electrodes in the presence of K_3/K_4 $[Fe(CN)_6]$ in PBS (pH 7.4) at a scan rate 50 mV s^{-1}. The formation of MPA thiol monolayer on the pristine Au electrode is indicated by the decreased anodic peak current (from 8.2 μA to 6.5 μA) and increased peak-to-peak separation ((ΔE_p) from 74 to 174 mV, curve b) compared to the bare electrode. Since the self-assembled MPA partially blocked the electron transfer reaction of $K_3/K_4[Fe(CN)_6]$, the peak separation was increased whereas the redox current was decreased. The lipid-CD-AgNPs tethering on the MPA monolayer further decreased the peak current from 6.5 to 4.4 μA and increased the peak-to-peak separation from 174 to 254 mV (curve c), confirming efficient attachment of lipid-CD-AgNPs on the MPA cushion layer. The R_{CT} of the MPA monolayer modified gold electrode is calculated to be 1.1×10^4 Ω cm^2. In corroboration with the CV data, the R_{CT} value of lipid-CD-AgNPs is increased to 3.2×10^4 Ω cm^2 from 1.1×10^4 Ω cm^2. These observations again indicate the effective attachment of lipid-CD-AgNPs on the MPA monolayer. The interaction of lipid with CD-AgNPs is investigated by monitoring the changes in zeta potential (ζ). The ζ value of cationic lipid DOTAP is 112.9 mV and the neutral zwitterionic lipid DOPE is ± 1.5 mV. The ζ of CD-Ag is −87.4 mV. The lipid-CD-AgNPs show ζ of 28.2 mV. The decreased ζ for the lipid-CD-AgNPs shows the effective interaction of CD-AgNPs with the lipid. The negative charge of the CD-AgNPs compensates the positive charge on the DOTAP lipid. In order to explore this further, surface coverage is calculated from the EIS data using the relation, $\theta_{IS}^{R} = 1-(R_{CT}^{Au}/R_{CT}^{SAM})$, proposed for partially covered monolayers (Wu et al., 2010). In this relation, θ_{IS}^{R} is the surface coverage. The θ_{IS}^{R} values less than 1 indicate the direct diffusion of K_3/K_4 $[Fe(CN)_6]$ to the free active sites on the gold surface through molecular defects like collapsed sites or pin holes. The θ_{IS}^{R} for the MPA monolayer modified gold surface is 0.9183. Higher value of θ_{IS}^{R} (0.9713) obtained for MPA-lipid-CD-AgNPs indicates the dense formation of lipid-CD-AgNPs on the MPA on gold electrode. This claim is further supported by the AFM study. Fig. 3A shows the AFM image of lipid-CD-AgNPs. The image is like an array with a particle size of 40 nm diameter and 40 nm height. This data is in corroboration with the particle size obtained from the HR-TEM (50 nm), as shown in Fig. 3B. The distribution of CDs in and around the lipid is witnessed by the appearance of black dots. The loading of CD-AgNPs inside the aqueous core and on the head groups of the lipid lead bigger sized nano particulates (Park et al., 2005).

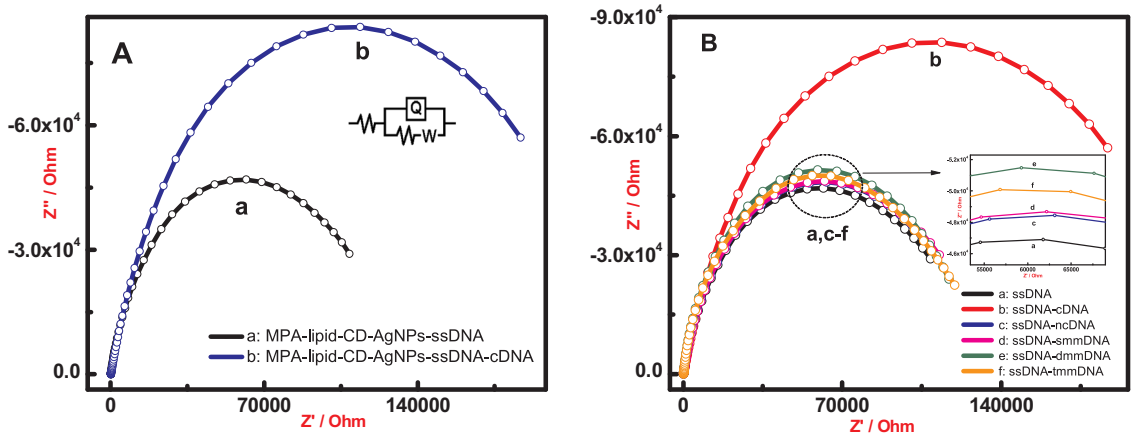

Fig. 4. (A) Impedance behaviors of MPA modified with lipid-CD-AgNPs-ssDNA surface for hybridization with target cDNA detection recorded in the frequency range 100 MHz to 0.1 Hz at an applied DC potential 160 mV in PBS buffer (pH 7.4) in the presence of 1 mM $K_3/K_4[Fe(CN)_6]$. The [R(Q(RW))] circuit fit data is given as open circles. (B) Comparative EIS behavior of MPA-lipid-CD-AgNPs-ssDNA (curve a) surface for hybridization with complementary DNA (curve b), non-complementary DNA (curve c), single base mismatch target DNA (curve d), double base mismatch target DNA (curve e) and triple base mismatch target DNA (curve f).

3.3. Electrochemical DNA mutation detection

The thiolated synthetic DNA representing lung cancer having 30 base pairs is immobilized on the lipid-CD-AgNPs through Ag-SH reaction. The attachment of DNA on the lipid-CD-AgNPs (ζ: 28.2 mV) reduces the ζ to 8.9 mV due to the negativity presence of negatively charged ssDNA. Since no significant change was observed from the voltammogram of $K_3/K_4[Fe(CN)_6]$, the more sensitive EIS technique is used for DNA hybridization sensing. Increased R_{CT} value of 1.13×10^5 Ω cm^2 is obtained following the immobilization of ssDNA due to electrostatic repulsion between the negatively charged DNA and $K_3/K_4[Fe(CN)_6]$. After the complementary target DNA hybridization on the MPA-lipid-CD-AgNPs -HS-ssDNA, the R_{CT} value is increased from 1.13×10^5 Ω cm^2 to 2.28×10^5 Ω cm^2 (Fig. 4A). The corresponding Q_{dl} value gets decreased after hybridization with cDNA (from 2.667×10^{-6} to 2.205×10^{-6} F cm^{-2}). This is due to the increased negative charge density on the electrode surface by hybridization and exertion of more electrostatic repulsion towards $K_3/K_4[Fe(CN)_6]$ complex. Absence of non-specific adsorption of HS-ssDNA on the surface is confirmed by the observation of insignificant change in both the R_{CT} and Q_{dl} for the experiments made without CD-AgNPs on the lipid, Fig. S7. Similar behaviors of these parameters are noticed in the experiment made using CD-AgNPs without lipid on the surface, Fig. S8. The hybridization of MPA- lipid-CD-AgNPs-ssDNA surface with the non-complementary target DNA (ncDNA) showed insignificant change in the R_{CT} value (from 1.13×10^5 Ω cm^2 to 1.16×10^5 Ω cm^2) indicating the high discrimination effect of this sensor surface. In order to demonstrate the high selectivity of the sensor, in addition to the non-complementary DNA (ncDNA), single base-mismatched (smmDNA), double base-mismatched (dmmDNA) and triple base-mismatch (tmmDNA) (mutated) target DNAs (Fig. 4B) were hybridized for which the R_{CT} values obtained are 1.22×10^5 Ω cm^2, 1.18×10^5 Ω cm^2 and 1.15×10^5 Ω cm^2, respectively. This confirms high selectivity of the sensor surface towards complementary DNA and mutated target DNAs. The CV also exhibits a similar behaviors for all hybridized surfaces, Fig. S6. The importance of the presence of lipid along with the CD-AgNPs on enhancing the DNA hybridization is also studied in the absence of lipid on the MPA layer, Fig. S7. The absence of lipid resulted in very minimal change of R_{CT} for the attachement of HS-ssDNA (0.8282×10^4 Ω cm^2) on the CD-AgNPs surface. Further, decreased EIS profile is observed for the complementary target DNA hybridization, Fig. S7. This is because of the fact that in the absence of lipid, the capture probe DNA may be attached in parallel orientation on the nanoparticle surface to prevent the direct diffusion of $K_3/K_4[Fe(CN)_6]$ for reaction on the free gold surface. Upon the target hybridization, the parallely oriented ssDNA may changes to the perpendicular orientation and allows free diffusion of $K_3/K_4[Fe(CN)_6]$ and lowers the EIS profile of the dsDNA compared to the EIS profile of ssDNA (Levicky et al., 1998). Another reason for this could be related to the basic nature of the CDs which stabilized the AgNP. The basic nature of CDs arises from the intrinsic oxygen functional groups present on the CDs (Zheng et al., 2015). The CDs is neutralized to pH 7 before its interaction with the lipid. In addition, the negative charge is partially reduced by its interaction with lipid and the ssDNA could be easily immobilized. Hence, the presence of liposome is essential for developing CDs based electrochemical DNA sensing platforms. A similar experiment is also performed for DNA sensing in the absence of CD-AgNPs (Fig. S8) and observed zero hybridization effect indicated by a nil change in the EIS signal before and after the target DNA hybridization. The stability of MPA-lipid-CD-AgNPs surface is investigated by preserving it at 4°C in the refrigerator for 8 days in PBS (pH 7.4) and recording the CV behavior on each day, Fig. S9. The peak current remains constant for the first two days and deteriorates slowly with time from third day. An intraday stability is also investigated by continuous potential cycling of the surface for 150 cycles at a constant scan rate of 50 mV s^{-1} for three times at different time intervals. It is noted that the sensor surface showed marginal decrease in the redox behavior of $K_3/K_4[Fe(CN)_6]$, indicating good stability of the sensing layer on the gold electrode. The effect of varying the target cDNA and ncDNA concentrations on the change of R_{CT} is evaluated using different concentrations of both complementary and non-complementary target DNAs on the MPA- lipid-CD-AgNPs-ssDNA. For each concentration, a separate electrode is used to avoid the use of NaOH or hot water for the dehybridizing the preformed dsDNA on the MPA-lipid-CD-AgNPs-ssDNA. The difference in the R_{CT} values obtained before and after target DNA (ΔR_{CT}) is used as a diagnostic parameter. A calibration curve is constructed by plotting ΔR_{CT} against target DNA concentrations (Fig. 5). The ΔR_{CT} linearly increases from 1×10^{-16} to 1×10^{-11} M while increasing complementary target DNA concentration, whereas the non-complementary DNA showed poor or negligible change in the R_{CT} with increasing target concentration. The accuracy and reliability of the sensor is compared by validating the present method with the standard spectrophotometric method, Table S1. It can be seen from the Table S1, the data obtained from the present study closely match with the results obtained from the spectrophotometry method. Error bar included in Fig. 5 is obtained for three repeated measurements and the calculated RSD is tabulated in Tables S2 and S3 for cDNA and ncDNA, respectively, for each concentration studied. The limit of detection (LOD) is determined following the IUPAC recommendation 1994,

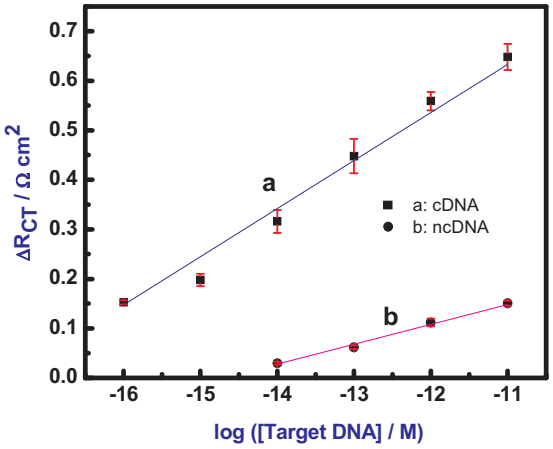

Fig. 5. Calibration curve showing change in charge transfer resistance (ΔR_{CT}) with complementary (curve a) and non-complementary (curve b) target DNA concentrations on the MPA-lipid-CD-AgNPs-ssDNA measured in presence of 1 mM $K_3/K_4[Fe(CN)_6]$ under similar conditions given in Fig. 4.

where the concentration of target DNA at the point intersection of the extrapolated linear range and the final lowest concentration level segment of the calibration plot (Buck and Lindner, 1994) is the LOD. From Fig. S10, the LOD value was calculated to be 10^{-16} M (Imran et al., 2018).

4. Conclusions

Silver nanoparticles stabilized carbon dots were synthesized and used to preserve the binary liposome vesicle formed using neutral (DOPE) and cationic (DOTAP) lipid. The presence of CD-AgNPs on the liposome stabilizes the vesicle structure, which was evidenced from the decreased zeta potential and increased particle size based on DLS and TEM measurements. Tethering of this complex on the monolayer modified gold electrode is confirmed by AFM and from the increased charge transfer resistance of the electrode. The essentiality of liposome presence along with CD-AgNPs is evidenced by the effective discrimination of single and complementary double stranded DNA by the lipid-CD-metal complex compared to the negligible discrimination noticed for the CD-AgNPs complex. That is, association of lipid with the CD-AgNPs is essential to enhance the amount of probe DNA attachment on the electrode inorder to increase the hybridization efficiency. The platform reported in this paper is selective and sensitive enough to detect DNA at concentrations below femtomole. The construction of this platform is easy and can be implemented for sensing application. Since Ag nanoparticle is used in this study, further investigations using other metal and/or metal oxides are essential to understand the role of metals on their stabilization with carbon dots for improving the sensing applications.

CRediT authorship contribution statement

Karutha Pandian Divya: Conceptualization, Methodology, Validation, Formal analysis, Writing - original draft, Writing - review & editing. **Rangasamy Karthikeyan:** Resources. **Bharathi Sinduja:** Resources. **Arockiajawahar Anancia Grace:** Resources. **S. Abraham John:** Resources, Writing - review & editing. **Jong Hoon Hahn:** Resources. **Venkataraman Dharuman:** Supervision, Project administration, Writing - review & editing.

Acknowledgements

Dr. Venkataraman Dharuman thanks the Department of Science and Technology, Science and Engineering Research Board (DST-SERB), India for the project support (DST-SERB, A13/DST-SERB/BE&BS/2015) and financial support by RUSA 2.0 [F.24-51/2014-U, Policy (TN Multi-Gen), Dept of Edn, Gol]. K.P. Divya thanks the Department of Science and Technology, India for the award of INSPIRE Fellowship (IF150890). Dr. S. Abraham John and B. Sinduja thank the Department of Science and Technology, Science and Engineering Research Board (DST-SERB) (EMR/2016/002898), India for the project support. J. H. Hahn thanks for the financial support from the Basic Science Research Program, the National Research Foundation of Korea (NRF) by the Ministry of Education (NRF-2018R1D1A1B07046959).

Declaration of interests

The authors declare that they have no known competing financial interests or personal relationships that could have appeared to influence the work reported in this paper.

Appendix A. Supporting information

Supplementary data associated with this article can be found in the online version at doi:10.1016/j.bios.2019.03.027.

References

Alfonta, L., Singh, A.K., Willner, I., 2001. Anal. Chem. 73, 91–102.
Bhunia, S.K., Saha, A., Maity, A.R., Ray, S.C., Jana, N.R., 2013. Sci. Rep. 3, 1473.
Buck, R.P., Lindner, E., 1994. Pure Appl. Chem. 66, 2527–2536.
Cagnin, S., Caraballo, M., Guiducci, C., Martini, P., Ross, M., SantaAna, M., Danley, D., West, T., Lanfranchi, T., 2009. Sensors 9, 3122.
Cailotto, S., Amadio, E., Facchin, M., Selva, M., Pontoglio, E., Rizzolio, F., Riello, P., Toffoli, G., Benedetti, A., Perosa, A., 2018. ACS Med. Chem. Lett. 9, 832–837.
Chen, B.S., Li, F.M., Li, S.X., Weng, W., Guo, H.X., Guo, T., Zhang, X.Y., Chen, Y.B., Huang, T.T., Hong, X.L., You, S.Y., Lin, Y.M., Zeng, K.H., Chen, S., 2013. Nanoscale 5, 1967–1971.
Chen, Z., Zhang, X., Yang, R., Zhu, Z., Chen, Y., Tan, W., 2011. Nanoscale 3, 1949–1956.
Dou, Q.Q., Fang, X.T., Jiang, S., Chee, P.L., Lee, T.C., Loh, X.J., 2015. RSC Adv. 5, 46817–46822.
El-Sayed, M.A., 2001. Acc. Chem. Res. 34, 257–264.
Gowthaman, N.S.K., Sinduja, B., Karthikeyan, R., Rubini, K., John, S.A., 2017. Biosens. Bioelectron. 94, 30–38.
Guo, R., Chen, B., Li, F., Weng, S., Zheng, Z., Chen, M., Wu, W., Lin, X., Yang, C., 2018. Sens. Actuator B: Chem. 264, 193–201.
Halder, A., Patra, S., Viswanath, B., Munichandraiah, N., Ravishankar, N., 2011. Nanoscale 3, 725–730.
Huang, Y., Shi, Y., Yang, H.Y., Ai, Y., 2015. Nanoscale 7, 2245–2249.
Imran, H., Manikandan, P.N., Dharuman, V., 2018. Sens. Actuator B: Chem. 260, 841–851.
Ivnitski, D., O'Neil, D.J., Gattuso, A., Schlicht, R., Calidonna, M., Fisher, R., 2003. Biotechniques 35, 682.
Jans, H., Huo, Q., 2012. Chem. Soc. Rev. 41, 2849–2866.
Jiang, D., Zhang, Y., Huang, M., Liu, J., Wan, J., Chu, H., Chen, M., 2014. J. Electroanal. Chem. 728, 26–33.
Kim, J., Park, J., Kim, H., Singha, K., Kim, W.J., 2013. Biomaterials 34, 7168–7180.
Kleinauskas, A., Rocha, S., Sahu, S., Sun, Y.-P., Juzenas, P., 2013. Nanotechnology 24, 325103.
Kudra, J., Richtera, L., Xhaxhiuc, K., Hynek, D., Heger, Z., Zitka, O., Adam, V., 2017. Biosens. Bioelectron. 15, 133–139.
Lermo, A., Campoy, S., Barbe, J., Hernandez, S., Alegret, S., Pividori, M.I., 2007. Biosens. Bioelectron. 22, 2010–2017.
Levicky, R., Herne, T.M., Tarlov, M.J., Satija, S.K.J., 1998. Am. Chem. Soc. 120, 9787–9792.
Li, F., Pei, H., Wang, L., Lu, J., Gao, J., Jiang, B., Zhao, X., Fan, C., 2013. Adv. Funct. Mater. 23, 4140–4148.
Li, H., Rothberg, L.J., 2004. Anal. Chem. 76, 5414–5417.
Li, H., Zhang, Y., Wang, L., Tian, J., Sun, X., 2011. Chem. Commun. 47, 961–963.
Li, J., Zhang, B., Wang, F., Liu, C.-Y., 2011. New J. Chem. 35, 554–557.
Loo, A.H., Sofer, Z., Bouša, D., Ulbrich, P., Bonanni, A., Pumera, M., 2016. ACS Appl. Mater. Interfaces 8, 1951–1957.
Lu, C.H., Yang, H.H., Zhu, C.L., Chen, X., Chen, G.N., 2009. Angew. Chem. Int. Ed. 121, 4879–4881.
Luo, P., Li, C., Shi, G., 2012. Phys. Chem. Chem. Phys. 14, 7360–7366.
Mao, G.-Y., Yang, W.-J., Bu, F.-X., Jiang, D.-M., Zhao, Z.-J., Zhang, Q.-H., Fang, Q.-C., Jiang, J.-S., 2014. J. Mater. Chem. B 2, 4481–4488.
Mao, X., Ma, Y., Zhang, A., Zhang, L., Zeng, L., Liu, G., 2009. Anal. Chem. 81, 1660.
Mondal, P., Ghosal, K., Bhattacharyya, S.K., Das, M., Bera, A., Ganguly, D., Kumar, P., Dwivedi, J., Gupta, R.K., Martí, A.A., Gupta, B.K., Maiti, S., 2014. RSC Adv. 4, 25863–25866.
Ostatna, V., Palecek, E., 2006. Langmuir 22, 6481.

Palchetti, I., Mascini, M., 2008. Analyst 133, 846.
Park, S.-H., Oh, S.-G., Mun, J.-Y., Han, S.-S., 2005. Colloid Surf. B 44, 117–122.
Peterson, A.W., Heaton, R.J., Georgiadis, R.M., 2001. Nucleic Acids Res. 29, 5163–5168.
Ping, J., Zhou, Y., Wu, Y., Papper, V., Boujday, S., Marks, R.S., Steele, T.W.J., 2015. Biosens. Bioelectron. 64, 373–385.
Pramanik, S., Chatterjee, S., Kumar, G.S., Devi, P.S., 2018. Phys. Chem. Chem. Phys. 20, 20476–20488.
Ray, S.C., Saha, A., Jana, N.R., Sarkar, R., 2009. J. Phys. Chem. C 113, 18546–18551.
Sachdev, A., Matai, I., Gopinath, P., 2015. J. Mater. Chem. B 3, 1217–1229.
Sharma, V.K., Yngard, R.A., Lin, Y., 2009. Adv. Colloid Interface Sci. 145, 83–96.
Sheila, N.B., Gary, A.B., 2010. Angew. Chem. Int. Ed. 49, 6726–6744.
Shen, J.H., Zhu, Y.H., Yang, X.L., Li, C.Z., 2012. Chem. Commun. 48, 3686–3699.
Steel, A.B., Levicky, R.L., Herne, T.M., Tarlov, M.J., 2000. Biophys. J. 79, 975–981.
Sun, X., Lei, Y., 2017. TrAC, Trends Anal. Chem. 89, 163–180.
Tang, L.B., Ji, R.B., Cao, X.K., Lin, J.Y., Jiang, H.X., Li, X.M., Teng, K.S., Luk, C.M., Zeng, S.J., Hao, J.H., Lau, S.P., 2012. ACS Nano 6, 5102–5110.
Tian, F., Lyu, J., Shi, J., Yang, M., 2017. Biosens. Bioelectron. 89, 123–135.
Tiwari, A., Gong, S., 2009. Talanta 77, 1217.
Varghese, N., Mogera, U., Govindaraj, A., Das, A., Maiti, P.K., Sood, A.K., Rao, C.N.R., 2009. ChemPhysChem 10, 206–210.
Wang, K., Ji, Q., Li, H., Guan, F., Zhang, D., Feng, H., Fan, H., 2017. J. Inorg. Biochem. 166, 64–67.
Wang, L., Luo, J., Shan, S., Crew, E., Yin, J., Zhong, C.-J., 2011. Anal. Chem. 83, 8688–8695.
Wang, Q., Song, H., Hu, Y., Su, Y., Lv, Y., 2014. RSC Adv. 4, 3992–3997.
Wang, Q., Wang, W., Lei, J., Xu, N., Gao, F., Ju, H., 2013. Anal. Chem. 85, 12182–12188.
Wilson, R., 2008. Chem. Soc. Rev. 37, 2028–2045.
Wu, J., Campuzano, S., Halford, C., Haake, D.A., Wang, J., 2010. Anal. Chem. 82, 8630–8837.
Xu, X., Ray, R., Gu, Y., Ploehn, H.J., Gearheart, L., Raker, K., Scrivens, W.A., 2004. J. Am. Chem. Soc. 126, 12736–12737.
Yang, R., Jin, J., Chen, Y., Shao, N., Kang, H., Xiao, Z., Tang, Z., Wu, Y., Zhu, Z., Tan, W., 2008. J. Am. Chem. Soc. 130, 8351–8358.
Yang, G., Zhu, C., Du, D., Zhu, J., Lin, Y., 2015. Nanoscale 7, 14217–14231.
Yang, Y., Asiri, A.M., Tang, Z., Du, D., Lin, Y., 2013. Mater. Today 16, 365–373.
Yang, Y., Cui, J., Zheng, M., Hu, C., Tan, S., Xiao, Y., Yang, Q., Liu, Y., 2012. Chem. Commun. 48, 380–382.
Yu, H., Zhang, H., Huang, H., Liu, Y., Li, H., Ming, H., Kang, Z., 2012. New J. Chem. 36, 1031–1035.
Yu, J., Xu, C., Tian, Z., Lin, Y., Shi, Z., 2015. New J. Chem. 40, 2083–2088.
Zhang, Y., Guo, Y., Xianyu, Y., Chen, W., Zhao, Y., Jiang, X., 2013a. Adv. Mater. 25, 3802–3819.
Zhang, Y., Xing, C., Jiang, D., Chen, M., 2013b. CrystEngComm 15, 6305–6310.
Zheng, X.T., Ananthanarayanan, A., Luo, K.Q., Chen, P., 2015. Small 11, 1620–1636.
Zhang, Y.-W., Li, H.-L., Sun, X.-P., 2011. Chin. J. Anal. Chem. 39, 998–1002.
Zheng, M., Liu, S., Li, J., Qu, D., Zhao, H.F., Guan, X.G., Hu, X.L., Xie, Z.G., Jing, X.B., Sun, Z.C., 2014. Adv. Mater. 26, 3554–3560.
Zhu, C., Zeng, Z., Li, H., Li, F., Fan, C., Zhang, H., 2013. J. Am. Chem. Soc. 135, 5998–6001.
Zhu, C., Zhai, J., Dong, S., 2012. Chem. Commun. 48, 9367–9369.
Zhu, Y.R., Ji, X.B., Pan, C.C., Sun, Q.Q., Song, W.X., Fang, L.B., Chen, Q.Y., Banks, C.E., 2013. Energy Environ. Sci. 6, 3665–3675.
Zhu, L., Cui, X., Wu, J., Wang, Z., Wang, P., Hou, Y., Yang, M., 2014. Anal. Methods 6, 4430–4436.